Inhomogeneity-Induced Casimir Transport of Nanoparticles

Fanglin Bao,[1] Kezhang Shi,[2] Guanjun Cao,[1] Julian S. Evans,[2] and Sailing He[2,1,3,*]

[1]*Centre for Optical and Electromagnetic Research, Guangdong Provincial Key Laboratory of Optical Information Materials and Technology, South China Academy of Advanced Optoelectronics, South China Normal University, Guangzhou 510006, China*

[2]*Centre for Optical and Electromagnetic Research, State Key Laboratory of Modern Optical Instrumentation, National Engineering Research Center of Optical Instrumentation, JORCEP, College of Optical Science and Engineering, Zhejiang University, Hangzhou 310058, China*

[3]*Department of Electromagnetic Engineering, Royal Institute of Technology, 10044 Stockholm, Sweden*

(Received 2 June 2017; published 24 September 2018)

We propose a scheme for transporting nanoparticles immersed in a fluid, relying on quantum vacuum fluctuations. The mechanism lies in the inhomogeneity-induced lateral Casimir force between a nanoparticle and a gradient metasurface and the relaxation of the conventional Dzyaloshinskiĭ-Lifshitz-Pitaevskiĭ constraint, which allows quantum levitation for a broader class of material configurations. The velocity for a nanosphere levitated above a grating is calculated and can be up to a few microns per minute. The Born approximation gives general expressions for the Casimir energy which reveal size-selective transport. For any given metasurface, a certain particle-metasurface separation exists where the transport velocity peaks, forming a "Casimir passage." The sign and strength of the Casimir interactions can be tuned by the shapes of liquid-air menisci, potentially allowing real-time control of an otherwise passive force, and enabling interesting on-off or directional switching of the transport process.

DOI: 10.1103/PhysRevLett.121.130401

Controlling nanoparticles is an essential tool that allows for an improved understanding of nanoscale interactions [1], development of self-assembly materials [2], labeled bioimaging [3], and photothermal nanomedicine [4]. Many techniques that rely on external fields such as optical tweezers [5], magnetic tweezers [6], thermal ratchets [7], etc., have been developed. However, passive systems that require no external input are much more efficient and fundamentally interesting for the development of complex lab-on-a-chip systems. Casimir forces arising from quantum vacuum fluctuations [8] are entirely internal to the system of interest and are thus an attractive candidate for developing passive "nanoparticle ramps."

The Casimir force has been experimentally measured to be consistent with theoretical predictions [9], and demonstrated in quantum actuation [10] to drive contactless nanodevices. Lateral Casimir forces that can affect fly-by nanoparticles have also been proposed recently, for a spinning particle near a plate (rotation-induced mirror-symmetry breaking) [11] and for an anisotropic particle near a plate in thermal nonequilibrium (anisotropy induced) [12]. To transport nanoparticles, contact friction from the substrate must be avoided through quantum levitation which, according to the Dzyaloshinskiĭ-Lifshitz-Pitaevskiĭ (DLP) constraint on the permittivities of the components [13,14], usually needs fluidic environments where previously reported mechanisms to generate lateral Casimir forces do not work [15].

This Letter proposes inhomogeneity-induced lateral Casimir forces, based on superhydrophobic gradient metasurfaces [16] as schematically shown in Fig. 1, and predicts the transport of an immersed nanoparticle driven by Casimir and/or Langevin stochastic forces. This transport process would generally be interrupted if either type of fluctuation is turned off in the Langevin equation, where quantum vacuum fluctuations generate a washboard-type Casimir energy ramp, while stochastic forces assist transitions of the nanoparticle to lower-energy positions across energy barriers. This behavior resembles a Brownian motor [17], and no external field is needed. For generic nanoparticles and gradient metasurfaces, Casimir energy barriers and directional lateral Casimir forces compete, yielding nontrivial transport velocity dependence on various parameters.

Considering a sphere of radius ρ above a one-dimensional grating of filling factor,

$$f(x)=\begin{cases} f_{\min} & \text{for } x\le 0 \\ f_{\min}+\frac{x(f_{\max}-f_{\min})}{L} & \text{for } 0<x<L \\ f_{\max} & \text{for } x\ge L, \end{cases} \tag{1}$$

where L is the length of a typical nanoparticle channel. The width of grooves of the grating w is kept constant, so that the sinking depth of the liquid-air menisci δ can be treated identically [period of unit cells is $p(x)=w/[1-f(x)]$]. The Casimir energy of this system at thermal equilibrium, in contrast to the well-known trace-log formula, evaluates the log operation and exactly reads [18]

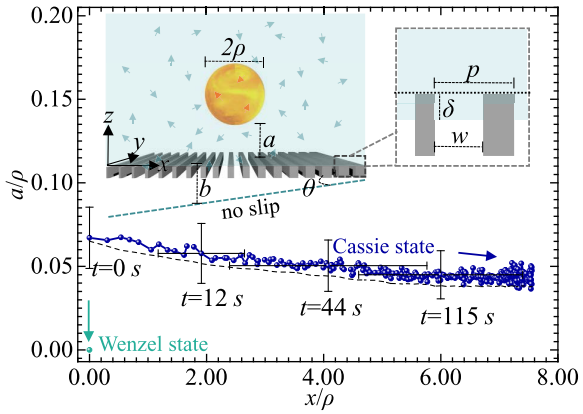

FIG. 1. Dynamics of a golden sphere ($\rho = 1$ μm) immersed in water above a one-dimensional silica grating ($f_{\min} = 0.001$, $f_{\max} = 0.5$, $L/\rho = 7.6$, $w/\rho = 0.1$) for Cassie ($\delta/w = 0$) and Wenzel states ($\delta/w = \infty$) at room temperature ($T = 300$ K). The dashed cyan curve below gratings and the dashed black curve below the trajectory represent the effective no-slip boundary and vertical equilibrium heights, respectively, for the Cassie state.

$$\mathcal{E} = \frac{-1}{\beta}\sum_{n=0}^{\infty}{}'\sum_{\gamma}\int_{-\infty}^{\infty}\langle \mathbf{k}\gamma, \mathrm{in}|\mathcal{X}\mathbb{R}_p\mathcal{X}\mathbb{R}_m|\mathbf{k}\gamma, \mathrm{in}\rangle_n d^2\mathbf{k}, \quad (2)$$

where $\beta = 1/k_B T$ (k_B the Boltzmann constant), $|\mathbf{k}\gamma, \mathrm{in}\rangle_n$ is the plane-wave state at a given Matsubara frequency $i\xi_n \equiv 2\pi n i/\hbar\beta$ ($\hbar$ the reduced Planck constant), $\mathbf{k}$ is the lateral wave vector in the x-y plane, $\gamma =$ TE or TM represents polarization, and in (out) means the negative- (positive-)z propagation direction. The prime on the summation over Matsubara frequencies indicates that the $n = 0$ term is weighted by $1/2$. And $\mathbb{R}_{p(m)}$ is the reflection operator of the nanoparticle (metasurface) to be evaluated at the $z = a$ (0) plane. $\mathcal{X} = e^{-\hat{k}_z a}$ is the translation operator where the normal wave number $k_z \equiv \sqrt{\mathbf{k}^2 + \varepsilon_f(\xi_n/c)^2}$ and $\varepsilon(\mathbf{r}, i\xi_n)$ is the permittivity at the corresponding Matsubara frequency (ε_f for the uniform fluid, c the speed of light in vacuum). Casimir forces $\mathcal{F}_j = -\partial_j\mathcal{E}$ have similar forms as Eq. (2), but with $\mathbb{R}_m$ replaced by

$$-\partial_j\mathbb{R}_m = \begin{cases} -i[\hat{\mathbf{k}}, \mathbb{R}_m]_- & \text{for } j = x, y \\ [\hat{k}_z, \mathbb{R}_m]_+ & \text{for } j = z, \end{cases} \quad (3)$$

where $[\cdot]_{-(+)}$ is the anticommutative (commutative) operator. For gradient metasurfaces, exact periodicity is lost in the unit-cell length scale but remains in the supercell length scale [16]. $\mathbb{R}_m$ can be evaluated by rigorous coupled-wave analysis [24], while $\mathbb{R}_p$ can be evaluated by partial-wave analysis [25,26].

Figure 2 shows $\mathcal{F}_j$ in the proposed system specified in Fig. 1, as functions of a/ρ, for varying δ/w and substrate materials. In the considered superhydrophobic case,

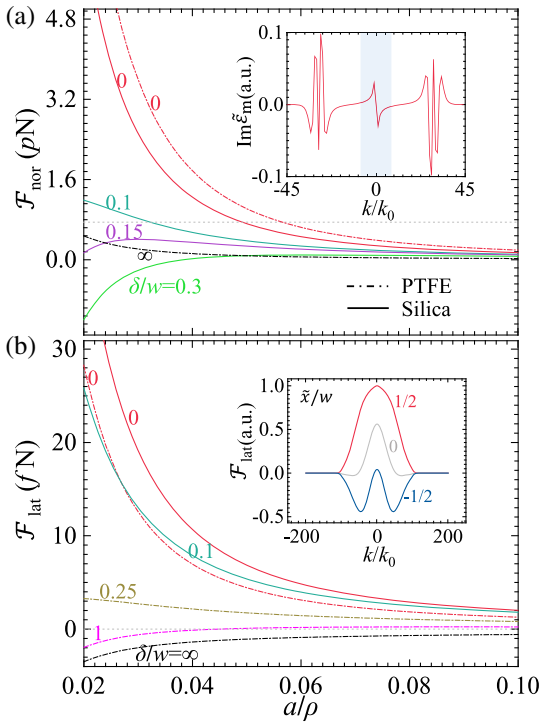

FIG. 2. (a) Normal and (b) lateral Casimir forces, $\mathcal{F}_{\mathrm{nor}}$ and $\mathcal{F}_{\mathrm{lat}}$, on the sphere described in Fig. 1 (at $x/\rho = 2.405$, center of a groove), as functions of particle-metasurface separation a/ρ, for varying sinking depths δ/w and substrate materials (fN: femto-Newton; pN: pico-Newton). $-G_z = 0.75$ pN is also shown in (a) (dotted gray line). Top inset: Profile of the imaginary part of the Fourier-transformed permittivity of a typical gradient metasurface at Matsubara frequencies. Bottom inset: Contributions of lateral wave number to $\mathcal{F}_{\mathrm{lat}}$ at different positions ($\tilde{x} = x - x_0$, $x_0/\rho = 5.045$ the center of a groove, $a/\rho = 0.02$). $k_0 = 2\pi/4.01$ μm.

water-silica and water-air interfaces both influence the sphere at a distance of a and $a + \delta$, respectively. For $\delta/w < 0.1$, the Au-water-silica (silica metasurface) configuration yields repulsive $\mathcal{F}_{\mathrm{nor}}$, which intersects with the $-G_z$ line (G represents classical forces including gravity and buoyancy), allowing levitation of the sphere. This also holds for Au-water-silicon and Au-water-Au configurations that have large Hamaker constants (not shown), as long as f is small enough. For $\delta/w > 0.15$, $\mathcal{F}_{\mathrm{nor}}$ exhibits nonmonotonicity [27], with a negative trend in the small-separation limit $a/\rho \to 0$, where $(a + \delta)/a$ becomes significant (influence of water-air interfaces significantly weakened as compared with that of water-silica interfaces). Water-polytetrauoroethylene (PTFE) interfaces repel the golden sphere as well as water-air interfaces, so no nonmonotonicity shows up when $\delta/w \to \infty$. From a macroscopic point of view, the above results mean that the total behavior of trapped air and substrate of the metasurface (ε_m) amounts to that of an effective planar medium ($1 < \varepsilon_{\mathrm{eff}} < \varepsilon_m$) [28], and thus the conventional DLP repulsion constraint $\varepsilon_m < \varepsilon_f < \varepsilon_p$ is significantly relaxed

to $\varepsilon_{\text{eff}} < \varepsilon_f < \varepsilon_p$. For gradient metasurfaces, mirror-symmetry breaking in the unit-cell length scale (captured by side peaks in the top inset) is common in previously studied periodic gratings, while symmetry breaking in the supercell length scale (shadowed peaks around $\pm k_0$ [29]) generates lateral inhomogeneity [30] that accounts for the inhomogeneity-induced lateral Casimir force. $\mathcal{F}_{\text{lat}}$ of magnitudes comparable with the particle's weight can also be analyzed via competing contributions from different interfaces. Notably, at a fixed particle position, $\mathcal{F}_{\text{lat}}$ from the PTFE metasurface flips sign for increasing δ, while $\mathcal{F}_{\text{lat}}$ from the silica metasurface remains directional. The Au permittivity in computations is obtained from a Drude model, $\varepsilon_{\text{Au}} = 1 + \Omega^2/\xi_n(\xi_n + \Gamma)$, with plasma frequency $\Omega = 1.28 \times 10^{16}$ rad/s and damping constant $\Gamma = 6.60 \times 10^{13}$ rad/s. The silica permittivity is fitted by Lorentz terms from tabular data [31]. Permittivities of water and PTFE are obtained from Lorentz models with parameters given in Ref. [32]. All magnetic responses are ignored.

These new features of Casimir forces lead to the ensemble-averaged trajectory ($\langle a(t)\rangle/\rho$ versus $\langle x(t)\rangle/\rho$) of the sphere in Fig. 1, according to the Langevin equation,

$$\dot{r}_i = \mu_{ij}[\mathcal{F}_j + G_j - m\ddot{r}_j] + \nu_{ij}\zeta_j(t), \tag{4}$$

where $\nu_{ij}\nu_{jk} = 2\mu_{ik}/\beta$ is implied by the fluctuation-dissipation theorem (μ_{ij} is the position-dependent mobility tensor), $-m\ddot{r}$ is the inertial force (dot means derivative with respect to time), and ζ with zero mean $\langle\zeta_i(t)\rangle = 0$, and temporal correlation $\langle\zeta_i(t)\zeta_j(t')\rangle = \delta_{ij}\delta(t - t')$ represents Gaussian white noise. The effective slip length of this system for the Cassie state ($\delta/w = 0$),

$$b(x) = \frac{p(x)}{2\pi}\ln\sec\left\{\frac{\pi}{2}[1 - f(x)]\right\}, \tag{5}$$

in comparison to uniform gratings [33], implies that the effective no-slip boundary is no longer parallel to the $z = 0$ plane due to gradients, but with an angle $\theta = \arctan\partial_x b$, and thus the mobility tensor generally features off-diagonal terms μ_{xz} and μ_{zx}. In the present case, θ is found to be within 4 deg for which off-digonal terms $\sim\sin\theta$ are vanishingly small, and thus lateral and normal motions of the sphere decouple. It turns out that different mobility profiles of $\mu_\parallel$ and $\mu_\perp$ do not alter our conclusions [34], and it is illustrative to model them as

$$\begin{aligned}\mu_\parallel &= \mu_0\left(1 - \frac{9}{16}\tau_\parallel + \frac{1}{8}\tau_\parallel^3 - \frac{45}{256}\tau_\parallel^4 - \frac{1}{16}\tau_\parallel^5 - \frac{83}{256}\tau_\parallel^6\right),\\ \mu_\perp &= \mu_0\left(1 - \frac{9}{8}\tau_\perp + \frac{1}{2}\tau_\perp^3 - 0.535\tau_\perp^4 + 0.160\tau_\perp^5\right),\end{aligned} \tag{6}$$

where $\tau_\perp = \rho/(\rho + a)$, $\tau_\parallel = \rho/(\rho + a + b)$, and μ_0 is the bulk mobility. Here it is further required that $\mu \to 0$ when $\tau \to 1$. The Cassie-state trajectory, obtained for 100 repeated finite-difference simulations for a total time of 270 s at a time step of $\delta t = 0.01$ s [35], illustrates the transport behavior with an average speed of about 2 μm/s. The Wenzel-state trajectory, on the other hand, drops immediately to around $a/\rho = 0$ and $x/\rho = 0$ from the beginning, as well as the case ignoring $\mathcal{F}_j$. If stochastic forces are turned off, the sphere (Cassie state) is found to travel along the equilibrium-height (dashed black) curve but gets stopped halfway by energy barriers (not shown). Diffusion makes $\langle a\rangle \equiv \int a\exp\{-\beta\mathcal{E}_{\text{tot}}\}da/\int\exp\{-\beta\mathcal{E}_{\text{tot}}\}da$ larger than the equilibrium height, where $\mathcal{F}_{\text{nor}} + G_z = 0$, due to the asymmetry of $\mathcal{E}_{\text{tot}}(a) = \mathcal{E}(a) - G_z a$ along the z direction. This quantitatively explains the fact that the Cassie-state trajectory in Fig. 1 is 5.8 nm above the equilibrium height. Tuning the sinking depth δ via pressure difference Δ of the liquid and air through the Young-Laplace equation $\delta \sim 2\Delta w^2/\sigma$ (σ the liquid-air surface tension) significantly affects the Casimir force (both sign and strength, see Fig. 2), and thus enables on-off or directional switching of the transport process.

More generally, mirror-symmetry breaking of the one-dimensional-gradient (along the x axis) metasurface could be approximated as (top inset of Fig. 2)

$$\begin{aligned}\text{Im}\tilde{\varepsilon}_m(k_x, i\xi_n) \approx &-q_1\text{sgn}(k_x)\delta\left(|k_x| - \frac{2\pi}{p}\right)\\ &- q_2\text{sgn}(k_x)\delta\left(|k_x| - \frac{2\pi}{P}\right),\end{aligned} \tag{7}$$

where P is the supercell dimension and $\text{Im}\tilde{\varepsilon}$ is the imaginary part of the Fourier transformed (in x axis; y and z dependences suppressed) permittivity. According to the Kramers-Kronig relation, $\varepsilon_m(\mathbf{r}, i\xi_n) = 1 + (2/\pi)\int_0^\infty \omega\text{Im}\varepsilon_m(\mathbf{r}, \omega)/(\omega^2 + \xi_n^2)d\omega$, q_1 and q_2 would always be zero if the mirror symmetry holds. Equation (7) corresponds to sinusoidally modulated permittivities, and under the Born approximation entails [36]

$$\mathcal{F}_{\text{lat}} = q_1 A\cos\left(\frac{2\pi}{p}x\right) + q_2 B \tag{8}$$

in the $P \gg x$ limit, which implies that the Casimir energy,

$$\mathcal{E}(x) = -q_1\frac{Ap}{2\pi}\sin\left(\frac{2\pi}{p}x\right) - q_2 Bx - C, \tag{9}$$

resembles a washboard-type potential ramp for the nanoparticle. Here, properties of the particle play their roles through A and B. The second term of Eq. (8) is the inhomogeneity-induced directional force, while the first term oscillates with x, qualitatively consistent with the bottom inset in Fig. 2 ($P = \tilde{P} = 4.01$ μm).

Figure 3 shows $v \equiv \dot{x}$ as a function of ρ/p, according to Eq. (9) and the overdamped Stratonovich formula [37],

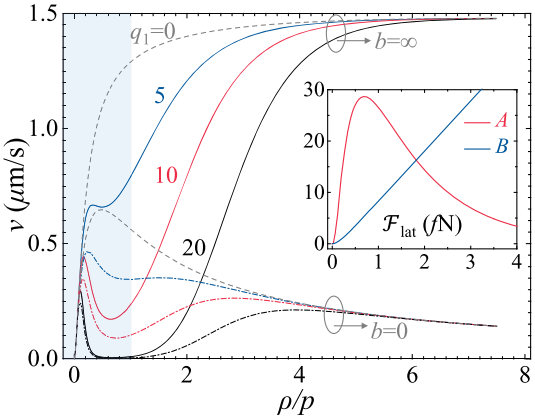

FIG. 3. Room-temperature Casimir transport velocity v as a function of radius ρ (normalized by $p = 200$ nm), for $a = 50$ nm, $P = 16.08$ μm, and $q_2 = 1$. Inset: A and B as functions of ρ/p.

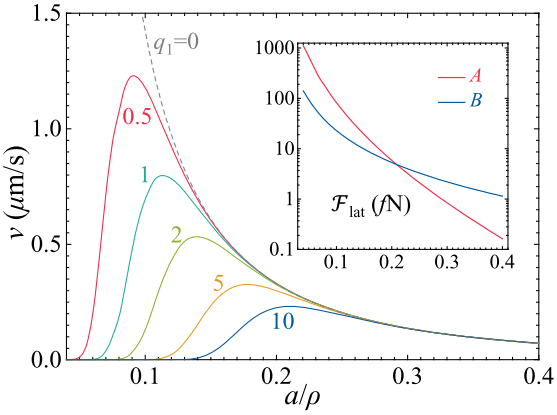

FIG. 4. Room-temperature Casimir transport velocity v as a function of separation a (normalized by $\rho = 500$ nm), for $b = \infty$, $q_2 = 1$, $p = 400$ nm, and $P = 16.08$ μm. Inset: A and B as functions of a/ρ.

$$v = \frac{p\mu_{\parallel}(1 - e^{-\beta q_2 B p})/\beta}{\int_0^p dx e^{-\beta\mathcal{E}(x)} \int_x^{x+p} dy e^{\beta\mathcal{E}(y)}}. \tag{10}$$

When $q_2 = 0$, Eq. (10) yields $v = 0$ and the proposed system recovers the interaction between a sphere and a periodic grating where Casimir transport does not occur. The asymptotic ($q_1 = 0$) velocity (dashed gray) in the $b = \infty$ limit, decreases rapidly when $\rho/p < 1$ and reaches a plateau when $\rho/p > 1$, due to the behavior of B/ρ. $B(\rho)$ (inset) is almost linear for large particle size, while $B = \mathcal{O}(\rho)$ when $\rho \to 0$. For nontrivial energy barriers (large q_1), the transport velocity shows a sharp peak in the $\rho/p < 1$ region (shadowed), increases rapidly in the $1 < \rho/p < 5$ range, and approaches the asymptotic plateau when $\rho/p > 5$, due to the behavior of A. For $\rho/p < 0.5$, both A and B increase with ρ, but A is much faster. For $\rho/p > 1$, force contributions from neighboring unit cells compete with each other and thus A decreases, leaving a peak around $0.5 < \rho/p < 1$, while B still increases. The nanoparticle is in the running state most of the time when $q_1 A$ is small, while it gets locked by energy barriers most of the time when $q_1 A$ becomes large. Therefore, the effective transport velocity is low in the region where A is large, and significantly deviates from the asymptotic curve. With increasing ρ/p the asymptotic velocity in the $b = 0$ limit increases rapidly at first but slowly decays later, due to the suppression of $\mu_{\parallel}$ by wall-induced hydrodynamic interactions [Eq. (6)]. Nontrivial energy barriers again result in sharp peaks of the velocity in the $\rho/p < 1$ region, indicating that the size-selective transport behavior is robust against the slippage of the metasurface. In all computations, A and B are generated assuming perfect conducting boundaries on the particle, for simplicity.

Competition between energy barriers (term A) and directional forces (B) results in an optimal value of a/ρ (Fig. 4). The asymptotic velocity (dashed gray) in the $b = \infty$ limit diverges when $a/\rho \to 0$ and decays when $a/\rho \to \infty$, similar to the behavior of the Casimir force $B(a)$. With any finite energy barrier, $v \to 0$ when $a/\rho \to 0$. As is shown in the inset, A diverges faster than B in the $a/\rho \to 0$ limit, and decays faster in the opposite limit. This means that, for any nonzero q_1, a finite a/ρ must exist below which energy barriers begin to dominate. The separation range around the velocity peak defines a priority passage for the nanoparticle, outside which nanoparticles are transported much slower, where smaller energy barriers result in narrower passages. The peaks are not around where $A \leq B$, so energy barriers are still important when v is optimized. The $b \to 0$ limit yields similar curves (not shown), indicating that those features are also robust against the slippage of the metasurface.

When the temperature of the system varies, Matsubara frequencies change and Casimir forces (both A and B) modestly increase with T (not shown). The total influence, according to Eq. (10), is that $v \propto 1/\beta \propto T$, which might be another way to control the transport.

In the proposed systems, Lewis acid-base interactions and electrostatic double-layer interactions are also present [38]. The former is usually within a range of 3 nm away from the plate, and the latter can be suppressed by using uncharged surfaces or tuning the Debye length to a similar range. Experiments have demonstrated pure Casimir effects without influence from those two interactions when the particle-metasurface separation is beyond 10 nm [13,39], and thus allow verification of the above results. The inhomogeneity-induced lateral Casimir force can also affect fly-by nanoparticles without fluidic environments. The Casimir transport and its velocity's dependence open new opportunities for developing technologies and explaining fundamental physical, biological, or chemical processes at the nanoscale.

This work was partially supported by China Postdoctoral Science Foundation (Grant No. 2017M622722), the National Key Research and Development Program of China (No. 2017YFA0205700), and the National Natural Science Foundation of China (No. 11621101).

*sailing@kth.se

[1] L. R. Liu, J. D. Hood, Y. Yu, J. T. Zhang, N. R. Hutzler, T. Rosenband, and K.-K. Ni, Science **360**, 900 (2018); D. S. Ether, Jr., L. B. Pires, S. Umrath, D. Martinez, Y. Ayala, B. Pontes, G. R. de S. Arajo, S. Frases, G.-L. Ingold, F. S. S. Rosa, N. B. Viana, H. M. Nussenzveig, and P. A. M. Neto, Europhys. Lett. **112**, 44001 (2015).

[2] D. Han, X. Qi, C. Myhrvold, B. Wang, M. Dai, S. Jiang, M. Bates, Y. Liu, B. An, F. Zhang, H. Yan, and P. Yin, Science **358**, eaao2648 (2017); S. Cheung and D. F. O'Shea, Nat. Commun. **8**, 1885 (2017).

[3] R. Diekmann, D. L. Wolfson, C. Spahn, M. Heilemann, M. Schttpelz, and T. Huser, Nat. Commun. **7**, 13711 (2016).

[4] D. Rosenblum, N. Joshi, W. Tao, J. M. Karp, and D. Peer, Nat. Commun. **9**, 1410 (2018); G. Xu, S. Zeng, B. Zhang, M. T. Swihart, K.-T. Yong, and P. N. Prasad, Chem. Rev. **116**, 12234 (2016).

[5] M. L. Juan, M. Righini, and R. Quidant, Nat. Photonics **5**, 349 (2011); O. M. Marago, P. H. Jones, P. G. Gucciardi, G. Volpe, and A. C. Ferrari, Nat. Nanotechnol. **8**, 807 (2013); L. Lin, M. Wang, X. Peng, E. N. Lissek, Z. Mao, L. Scarabelli, E. Adkins, S. Coskun, H. E. Unalan, B. A. Korgel, L. M. Liz-Marzn, E.-L. Florin, and Y. Zheng, Nat. Photonics **12**, 195 (2018).

[6] M. Wu, R. Yadav, N. Pal, and H. P. Lu, Rev. Sci. Instrum. **88**, 073703 (2017).

[7] M. O. Magnasco, Phys. Rev. Lett. **71**, 1477 (1993); S.-H. Wu, N. Huang, E. Jaquay, and M. L. Povinelli, Nano Lett. **16**, 5261 (2016).

[8] *Casimir Physics*, Lecture Notes in Physics, Vol. 834, edited by D. R. D. Dalvit, P. Milonni, and F. da Rosa (Springer, Berlin, 2011); A. W. Rodriguez, F. Capasso, and S. G. Johnson, Nat. Photonics **5**, 211 (2011).

[9] U. Mohideen and A. Roy, Phys. Rev. Lett. **81**, 4549 (1998).

[10] H. B. Chan, V. A. Aksyuk, R. N. Kleiman, D. J. Bishop, and F. Capasso, Science **291**, 1941 (2001).

[11] A. Manjavacas, F. J. Rodríguez-Fortuño, F. J. García de Abajo, and A. V. Zayats, Phys. Rev. Lett. **118**, 133605 (2017).

[12] B. Müller and M. Krüger, Phys. Rev. A **93**, 032511 (2016).

[13] J. N. Munday, F. Capasso, and A. Parsegian, Nature (London) **457**, 170 (2009).

[14] A. W. Rodriguez, M. T. Homer Reid, F. Intravaia, A. Woolf, D. A. R. Dalvit, F. Capasso, and S. G. Johnson, Phys. Rev. Lett. **111**, 180402 (2013).

[15] Lateral Casimir forces arising from displacement-induced mirror-symmetry breaking cannot lead to net transport of nanoparticles, but can serve in a time-correlated ratchet; see T. Emig, Phys. Rev. Lett. **98**, 160801 (2007).

[16] See, e.g., T. Liu and C.-J. Kim, Science **346**, 1096 (2014) for superhydrophobicity; see, e.g., F. Ding, A. Pors, and S. I. Bozhevolnyi, Rep. Prog. Phys. **81**, 026401 (2018) for a review of gradient metasurface.

[17] R. D. Astumian and P. Hänggi, Phys. Today **55**, No. 11, 33 (2002); P. Hänggi and F. Marchesoni, Rev. Mod. Phys. **81**, 387 (2009).

[18] See Supplemental Material at http://link.aps.org/supplemental/10.1103/PhysRevLett.121.130401, which includes Refs. [19–23], for the derivation.

[19] B. A. Lippmann and J. Schwinger, Phys. Rev. **79**, 469 (1950).

[20] J. Happel and H. Brenner, *Low Reynolds Number Hydrodynamics with Special Applications to Particulate Media* (Martinus Nijhoff Publishers, The Hague, 1983).

[21] O. Kenneth and I. Klich, Phys. Rev. Lett. **97**, 160401 (2006).

[22] O. Kenneth and I. Klich, Phys. Rev. B **78**, 014103 (2008).

[23] A. L. Dubov, S. Schmieschek, E. S. Asmolov, J. Harting, and O. I. Vinogradova, J. Chem. Phys. **140**, 034707 (2014).

[24] P. S. Davids, F. Intravaia, F. S. S. Rosa, and D. A. R. Dalvit, Phys. Rev. A **82**, 062111 (2010); For details about how RCWA is applied to gradient metasurfaces, see Supplemental Materials http://link.aps.org/supplemental/10.1103/PhysRevLett.121.130401.

[25] P. A. M. Neto, A. Lambrecht, and S. Reynaud, Phys. Rev. A **78**, 012115 (2008); S. J. Rahi, T. Emig, N. Graham, R. L. Jaffe, and M. Kardar, Phys. Rev. D **80**, 085021 (2009); A. Canaguier-Durand, P. A. M. Neto, I. Cavero-Pelaez, A. Lambrecht, and S. Reynaud, Phys. Rev. Lett. **102**, 230404 (2009).

[26] R. Messina, P. A. Maia Neto, B. Guizal, and M. Antezza, Phys. Rev. A **92**, 062504 (2015).

[27] Nonmonotonic Casimir forces have been experimentally observed between intersecting nanostructures; see L. Tang, M. Wang, C. Y. Ng, M. Nikolic, C. T. Chan, A. W. Rodriguez, and H. B. Chan, Nat. Photonics **11**, 97 (2017).

[28] The valid expression of $\varepsilon_{\mathrm{eff}}$ in Casimir problems is beyond the scope of this Letter. For various effective medium approximations, see, e.g., A. Azari, M. F. Miri, and R. Golestanian, Phys. Rev. A **82**, 032512 (2010); R. Esquivel-Sirvent and G. C. Schatz, Phys. Rev. A **83**, 042512 (2011); G. Song, J. Xu, C. Zhu, P. He, Y. Yang, and S.-Y. Zhu, Phys. Rev. A **95**, 023814 (2017).

[29] k_0 comes from the reconstruction technique. See Supplemental Material at http://link.aps.org/supplemental/10.1103/PhysRevLett.000.000000, Sec. SII, for further details.

[30] The Casimir effect within an inhomogeneous system has been investigated previously; see, e.g., F. Bao, B. Luo, and S. He, Phys. Rev. A **91**, 063810 (2015); F. Bao, J. S. Evans, M. Fang, and S. He, Phys. Rev. A **93**, 013824 (2016).

[31] E. D. Palik, *Handbook of Optical Constants of Solids* (Academic Press, New York, 1985).

[32] P. J. van Zwol and G. Palasantzas, Phys. Rev. A **81**, 062502 (2010).

[33] A. V. Belyaev and O. I. Vinogradova, J. Fluid Mech. **652**, 489 (2010).

[34] See Supplemental Material at http://link.aps.org/supplemental/10.1103/PhysRevLett.121.130401, Sec. SIII, for further details.

[35] The trajectory is shown with $\delta t = 1$ s rather than 0.01 s, where the transport velocity can be revealed from the data density.

[36] Derivations are quite similar to the case of sinusoidally corrugated surfaces; see, e.g., D. A. R. Dalvit, P. A. M. Neto, A. Lambrecht, and S. Reynaud, J. Phys. A **41**, 164028 (2008).

[37] B. Lindner, M. Kostur, and L. Schimansky-Geier, Fluctuation Noise Lett. **01**, R25 (2001).

[38] C. J. van Oss, J. Mol. Recognit. **16**, 177 (2003).

[39] R. F. Tabor, R. Manica, D. Y. C. Chan, F. Grieser, and R. R. Dagastine, Phys. Rev. Lett. **106**, 064501 (2011).